Phase Diagram of $RAgSb_2$ (R=Y, La, Gd) and (Magneto)Thermoelectric effects in Fe_3GeTe_2

Aaron Breidenbach,* Anna Roche,† Joshua Mutch,† Joshua Sanchez,† and Jiun-Haw Chu†
(University of Washington Physics REU Program)
(Dated: August 24, 2018)

This paper focuses on two separate projects completed by the author as part of a ten week National Science Foundation Research Experience for Undergraduates (REU) program. The first section focuses on the measurement of the phase diagram of $RAgSb_2$ (R=Y,La,Gd), which is of particular interest, as doping from R=La to R=Gd is likely to create two quantum critical points related to charge density waves and antiferromagnetic states. Such quantum critical points have been linked to high temperature superconductivity in cuprates such as $YBa_2Cu_3O_{7-x}$ (YBCO) but isn't well understood theoretically, so the study of the similar $RAgSb_2$ crystals may lead to further insights about the superconducting mechanism in the cuprates. Part of this phase diagram has been determined, and no superconducting phase of $RAgSb_2$ has been found yet, but further doped crystals with finer spacing need to be grown to resolve the quantum critical points of interest. In the second section, (magneto)thermoelectric coefficient measurement is motivated as a probe of a material's density of states at the Fermi energy, which could be particularly interesting for novel materials with large Berry Curvatures such as Fe_3GeTe_2. Such (magneto)thermoelectric measurements of bulk crystals may be possible through the extension of a technique developed for the thermoelectric measurement of epitaxial thin films developed in previous work at the University of Minnesota. This potential extension, preliminary successes, and the issues encountered while working towards this are discussed, although quantitative results are still forthcoming.

I. OVERVIEW

Throughout this ten week REU program, I have had the pleasure of working on two distinct and separate research projects in Professor Jiun-Haw Chu's Quantum Materials Laboratory. While we have learned a lot through working on both projects, they are fairly unrelated so I introduce and discuss each topic separately.

In section II I discuss the measurement of the phase diagram of $RAgSb_2$ (R=Y, La, Gd) and the potential emergence of superconductivity.

After that, in section III, I introduce separately the measurement of and motivation behind (magneto)thermoelectric coefficient measurements, much of which is based research I have previously completed in Paul Crowell's spin dynamics and transport group at the University of Minnesota.

Finally, in section IV I summarize and conclude what we have learned throughout the course of this summer.

II. PHASE DIAGRAM OF, AND POTENTIAL SUPERCONDUCTIVITY IN $RAgSb_2$ (R=Y, La, Gd)

A. Introduction

Superconductors (SCs) are much sought after materials having a wide variety of applications in industry and the experimental sciences, ranging from magnetic resonance imaging (MRI) machines in medicine, to fast magnetically levitating (Maglev) trains, to high sensitivity particle detectors in experimental physics. Due to their wide variety of applications, it is desirable to find new, accessible, superconducting materials with higher critical temperatures, so that they may be cheaply available and cooled with relatively affordable liquid nitrogen (LN_2) rather than liquid helium.

While some LN_2 temperature superconductors have been found in the form of cuprates such as $YBa_2Cu_3O_{7-x}$ (YBCO), the mechanism behind this high temperature superconducting phase is not well described by traditional Bardeen-Cooper-Schrieffer (BCS) superconductivity theory [1]. Additionally, many high temperature SCs such as YBCO are brittle and not suitable for many applications because of this.

This motivates looking for superconductivity in $RAgSb_2$ as it shares similar phases of matter and a similar quasi-2D electronic structure with the cuprates that may also lead to a high temperature superconducting phase (see section II B). Even if such a SC phase in $RAgSb_2$ is not found, it will demonstrate that despite being a similar system to the cuprates, something must be different such that the emergent SC phase is suppressed. Information like this will be useful as non-BCS theories are developed to explain high temperature superconductivity in exotic materials such as YBCO, which makes $RAgSb_2$ worthwhile to study.

* Physics Department, University of Minnesota
† Physics Department, University of Washington

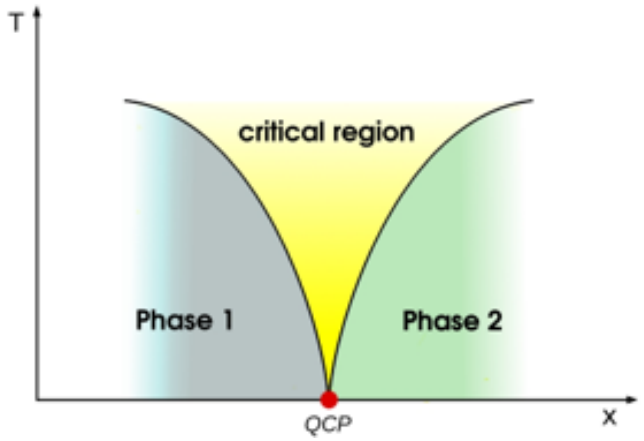

FIG. 1: Cartoon illustrating the qualitative features of a quantum critical point. A phase transition occurs at absolute zero temperature as a different quantity x is varied, which can result in exotic phases in the critical region. Graphic courtesy Inspire HEP.

B. Theory

In the high temperature SCs such as YBCO, the superconducting phase is known to occur near, and is most likely related to, a quantum critical point (QCP) in its phase diagram [1]. As is shown in Fig. 1, a QCP is a continuous phase transition between two generic states of matter that occurs at absolute zero in temperature when a different quantity x is varied. While the quantity x can generically be many things (i.e. magnetic field or pressure) in the case of the SC cuprates, this quantity is percent chemical doping. Specifically, from observing Fig. 2, the high temperature SC phase occurs near the QCPs associated with the complete suppression of the charge density wave (CDW) and antiferromagnetic (AFM) states as a function of oxygen doping [3].

In $RAgSb_2$, the parent compound $LaAgSb_2$ is known to have a CDW transition at 212K, while the parent compound $GdAgSb_2$ is known to have an AFM transition at 13K [4]. Meanwhile the parent compound $YAgSb_2$ is a metallic paramagnet which has no low temperature phase transitions [4]. This means that by doping one of these compounds into another, one would expect the unique phase of the parent compound to be suppressed with doping creating four quantum critical points in the phase diagram as is illustrated by the qualitative schematic in Fig. 3. Additionally the choice of these compounds is deliberate such that the AFM and CDW QCPs are realized when doping from Gd to La in $RAgSb_2$ so that the QCPs near the high temperature SC phase in Fig. 2 may be replicated, while the Y-doping is used primarily as a control to see if SC behavior may also be realized at other types of QCPs. $RAgSb_2$ also has a layered tetragonal crystal structure, as shown in Fig. 4, meaning it shares crystal lattice symmetry and a quasi-2D electronic structure with the cuprates, further motivating its study [5].

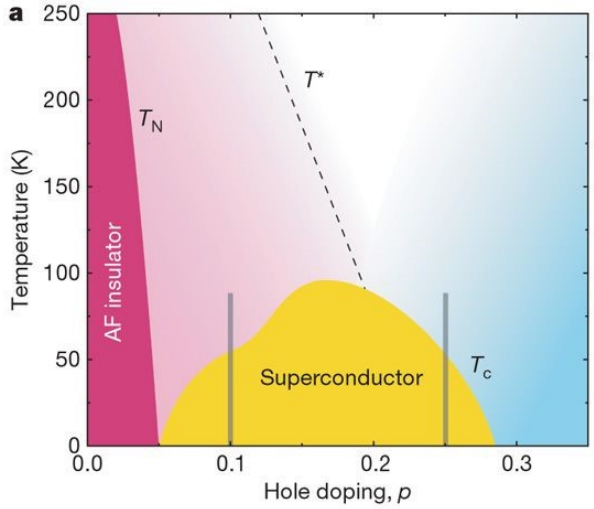

(a) Phase diagram of the cuprate compound $YBa_2Cu_3O_{7-x}$ (YBCO). The high temperature superconducting phase occurs near quantum critical points associated with the suppression of the antiferromagnetic and charge density wave states as a function of (oxygen) hole doping. Figure from Doiron-Leyraud et. al. [1].

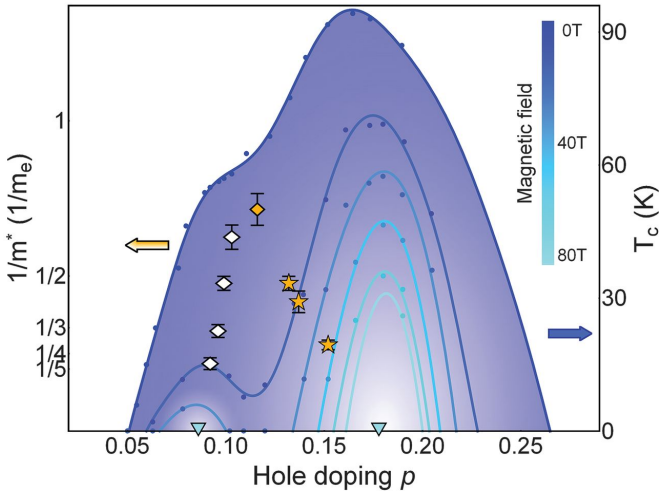

(b) Superconducting transition of YBCO as a function of applied magnetic field and hole doping, showing that the superconducting phase has a maximum enhancement at p≈0.18, which corresponds to the quantum critical point where the CDW state is suppressed. Figure from Ramshaw et. al. [2]

FIG. 2

C. Crystal Growth

To grow the $RAgSb_2$ crystals (whose layered structure is shown in Fig. 4) at various doping levels, a flux growth technique based off of Ref. [4] is used. This technique involves placing the reactants in a crucible in a non-stoichiometric ratio of $R_{0.045}Ag_{0.091}Sb_{0.864}$ so that excess Sb can be used as a self-flux, while the additional silver helps prevents the unwanted formation of the side com-

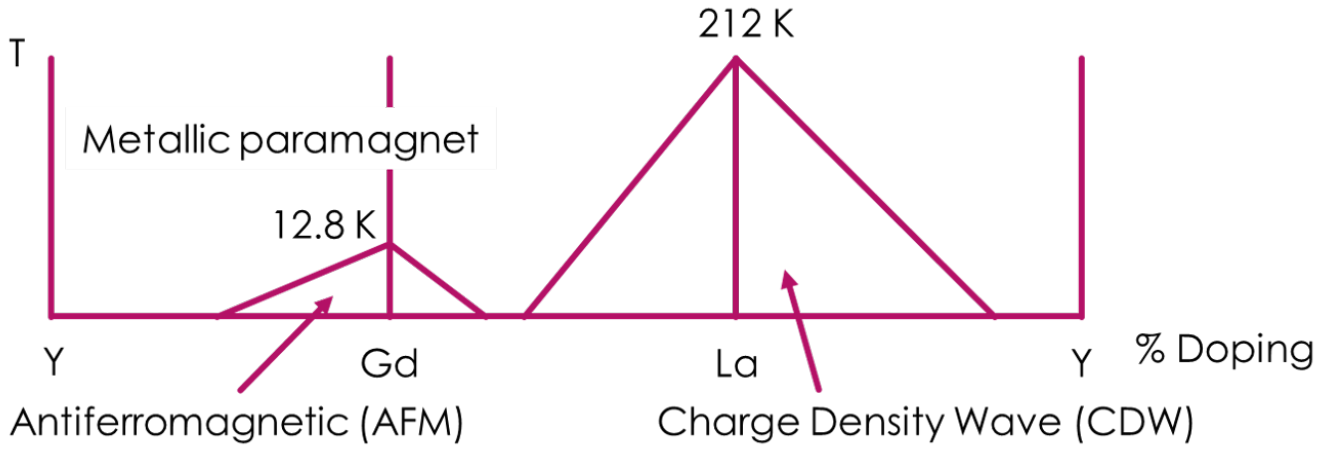

FIG. 3: An expected qualitative phase diagram of $RAgSb_2$ based off the known phases of the parent compounds. Note that four quantum critical points are expected to occur, including two involving the suppression of antiferromagnetic and charge density wave states that may arise in superconductivity similar to that seen in cuprates such as $YBa_2Cu_3O_x$ (YBCO).

pound RSb_2. This crucible is then vacuum sealed in a glass tube. The sealed crucible is heated to temperatures of ∼1200C and cooled over a week-long period to a final temperature of ∼400C to allow crystal formation. At ∼400C the sealed crucible is removed and quickly flipped over and centrifuged to allow the molten Sb flux to be filtered out, leaving behind plate-like single crystals, as shown in Fig. 5, where the c-axis (see Fig. 4) is out of plane.

D. Crystal Processing

After the crystals are grown using the techniques detailed in section II C, they must be processed from their plate-like form in Fig. 5 into a long and thin rectangular bar before measurements of the phase diagram may be preformed. While this may seem trivial in principle, in practice $RAgSb_2$ crystals are difficult to process due to their propensity to break and crumble, which is a large part of the reason they have yet to be measured. As such, much of my work in this REU program was focused on the processing of these crystals into precise rectangular shapes so quality phase transition data could be achieved. One of the lasting contributions I made to the Chu lab this summer was the creation of a standard operating procedure on how to produce such crystals, so I give a brief summary of how this is accomplished below.

The first step in the processing of these crystals involves cutting a thin strip of this material parallel to the ab plane of the crystal. This can be accomplished with a Princeton Scientific Corp. Precision Wire Saw (Model:WS25). The alignment of the cut with the crystal axes is important, so extra care must be taken to ensure this alignment is precise.

The process of doing this involves first mounting a sheet of the crystal on a microscope slide with Crystalbond glue so that its face is parallel to the ab plane of the crystal. This slide is then mounted on the wire saw stage, using a specially machined block to ensure that orthogonality is maintained through the process. The rotation of the stage is then carefully adjusted to ensure the cutting wire is parallel to the microscope slide (and therefore the ab plane). The cut is made after this alignment is complete to obtain a thin (∼20μm) slice of the crystal. This thin slice is then cut into a rectangular piece using similar methods to ensure the orthogonality of the cuts.

Once a rectangular piece of crystal is obtained, it is masked with paper and sputtered with gold in order to make contact points. These contact points can then be connected to gold wires with silver paste in order to allow connections for measurements to be made.

E. Measurement

Once the processing of these devices is complete, the measurement of the phase transition itself is straightforward. Since all of the phase transitions expected in these crystals would involve some change in electronic ordering (see Fig. 3 for expected phases), there will be an abrupt change in the resistance of a material at the phase transition temperature as the resistance will be affected by the change in electronic ordering. Therefore, when the resistance is plotted as a function of temperature for a given crystal, one expects to see a discontinuity in the derivative at the phase transition temperature, as is shown in Fig. 6.

Technically, more information is required to determine the exact phase before and after the transition, as all generic transitions affecting electronic ordering would result in this discontinuity. However, given that the phases

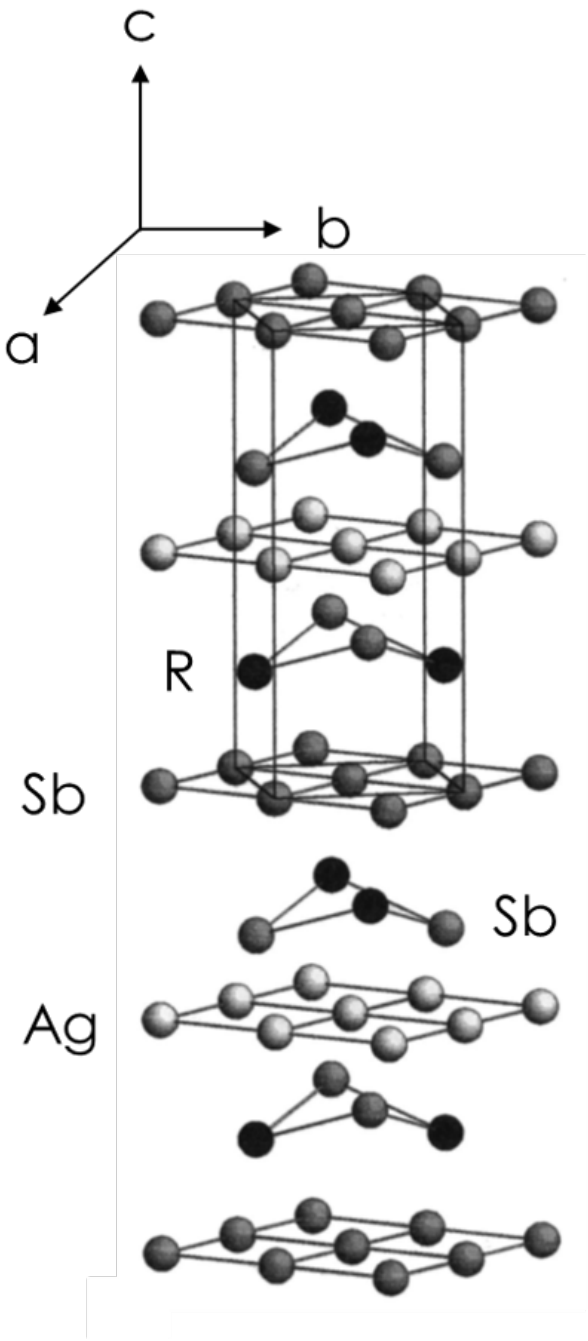

FIG. 4: Layered crystal structure of $RAgSb_2$ with principle crystal axes labeled. Figure from Myers et. al. [4].

and transition temperatures of the parent compounds are known *a priori* [4], the phases of the doped compound can be inferred quite easily, at least in an informal matter. In the case of an ambiguity, it is possible to unambiguously resolve the phases using other experimental techniques. CDWs can be imaged using x-ray diffraction [6], while the AFM and paramagnetic states can be observed directly using magnetic susceptibility or neutron scattering measurements. Such measurements have not been preformed on the present crystals, but are mentioned for the sake of completeness.

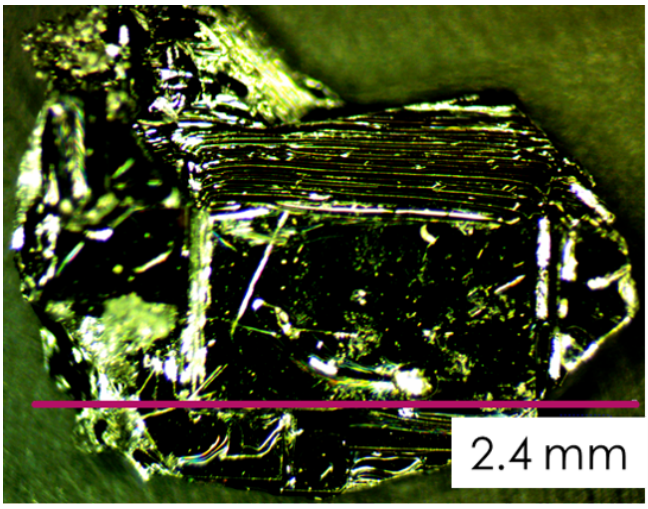

FIG. 5: An example $RAgSb_2$ crystal formed from a flux growth (specifically $Y_{0.55}Gd_{0.45}AgSb_2$). The c-axis is normal to the plated sheets that form (see Fig. 4).

F. Results and Discussion

Using the techniques of section II E, the phase transitions of fourteen differently doped $RAgSb_2$ compounds were measured and are summarized in Fig. 7. The majority of these measurements and analysis was completed by fellow undergraduate Anna Roche, who deserves due credit for the data presented here. This phase diagram shows the suppression of the CDW and AFM states as dopants are respectively introduced to the $LaAgSb_2$ and $GdAgSb_2$ parent compounds, as expected. While no emergent SC phase has been found yet, there remains much space to be covered on the phase diagram. Many other materials have narrow SC doping ranges ($BaFe_{2-x}Co_xAs_2$ for example [7]), so it is remains possible that an SC phase could yet be uncovered in $RAgSb_2$. Specifically, more $La_xGd_{1-x}AgSb_2$ crystals in the x=0-0.25 range should be grown in order to search for the QCPs at which full suppression of the CDW and AFM states are achieved. It is also possible that there is no QCP in $La_xGd_{1-x}AgSb_2$, but instead a coexistence of the CDW and AFM states or a first order quantum phase transition, further motivating the growth of these finer dopings in order to resolve this. Additionally, crystals of $La_xY_{1-x}AgSb_2$ should be grown in order to find the CDW to metallic paramagnet QCP and round out the phase diagram.

There exist a few avenues for further research on the $RAgSb_2$ crystals beyond adding additional points to the phase diagram in Fig. 7. One such avenue would be

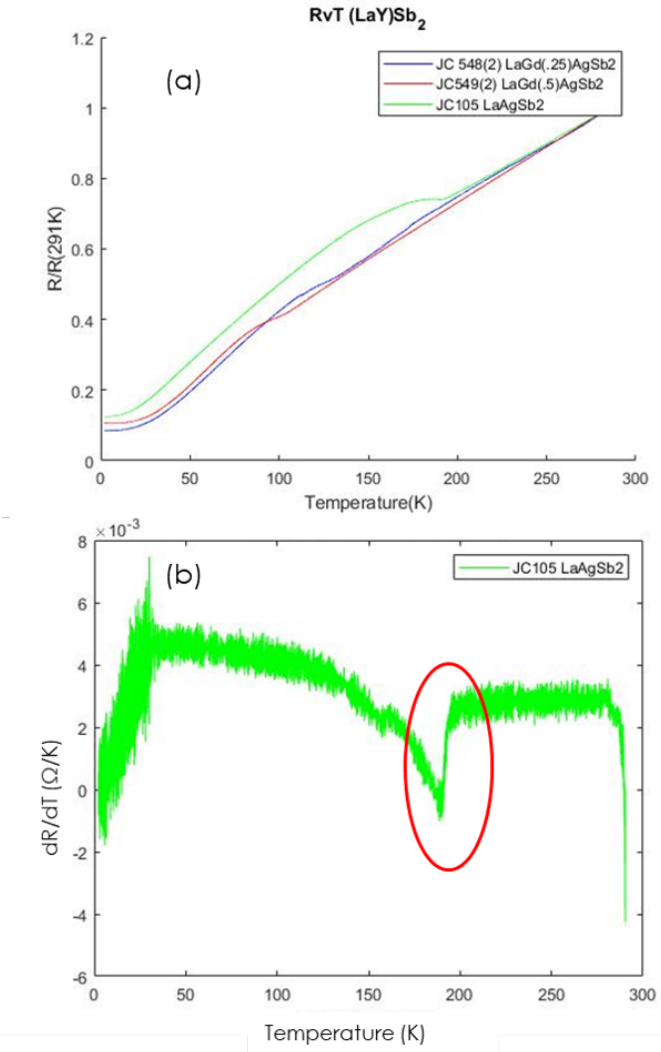

FIG. 6: (A) Resistance vs temperature plots for a few $RAgSb_2$ crystals. The kinks in this plot represent a phase transition that affects electronic ordering. (B) A derivative plot of dR/dT for $LaAgSb_2$. The discontinuity in this derivative can be used to precisely define the phase transition temperature.

adding Pd and Ni dopants in place of the Ag in this crystal. SC phases have been observed in both $LaPdSb_2$ and $LaNiSb_2$ crystals, so it could be interesting to see how the rare earth doping affects this transition [8]. Another avenue would involve adding Bi dopant in place of the Sb. Bi is nearly chemically identical to Sb, but is a much larger ion, so it would have the effect of stretching the lattice without changing its electronic properties. This would affect the spacing of the CDW state and could change properties of the phase transitions as well.

III. (MAGNETO)THERMOELECTRIC EFFECTS IN FE_3GETE_2

A. Theory

The Seebeck effect is the phenomenon by which an applied temperature gradient will result in a voltage gradient along the same direction. In understanding this effect, it is helpful to remember that that charge carriers are particles that will be affected and transported by chemical potentials in addition to voltage gradients. Ohm's law can then be generalized to include temperature gradients

$$J_\alpha = \sigma_{\alpha\beta}(\partial_\beta V - S_{\beta\gamma}\partial_\gamma T). \tag{1}$$

In the open circuit configuration, in which J=0, this leads to a simple definition of the Seebeck Coefficient S=S_{xx}:

$$S = -\frac{\Delta V}{\Delta T}. \tag{2}$$

Generally, the off diagonal elements of the Seebeck Tensor of Eq. 1 will be zero, unless some component such as a magnetization or magnetic field is present to break time reversal symmetry, analogous to the conductivity tensor's off diagonal elements. When such a symmetry breaking component is present, the Seebeck tensor allows for transverse voltage responses, which are collectively termed Nernst effects. These are analogous to the more familiar family of Hall Effects that occur when running current through a material in the presence of magnetization or a magnetic field. As such, the anomalous Nernst effect is the process by which a transverse voltage builds up across a magnetized sample when a temperature gradient is applied across it. The anomalous Nernst coefficient is then defined as [9]

$$S^A_{xy} = \frac{-\Delta V}{w * \partial_x T}\frac{M_s}{M_z}, \tag{3}$$

where w is the width of the sample, M_z is the out of plane component of the magnetization, M_s is the saturation magnetization of the magnetic film, and the superscript A is used to refer to the anomalous portion of the Nernst coefficient which is caused by the presence of magnetization (as opposed to the ordinary Nernst coefficient, which is related to applied magnetic fields). The importance of the Nernst coefficient comes from its relation to the anomalous Hall conductivity (AHC) and the band structure of a material [10],

$$S^A_{xy}\sigma_{xx} = \frac{\pi^2 k_b^2 * T}{3e}\frac{d\sigma^A_{xy}(\mu)}{dE}, \tag{4}$$

where σ^A_{xy} is the AHC, and μ is the Fermi Level. It should be emphasized in Eq. 4 that the Nernst coefficient is proportional to the energy derivative of the AHC at the Fermi level. The AHC is proportional to the spin-resolved density of states (DOS) at the Fermi level, so

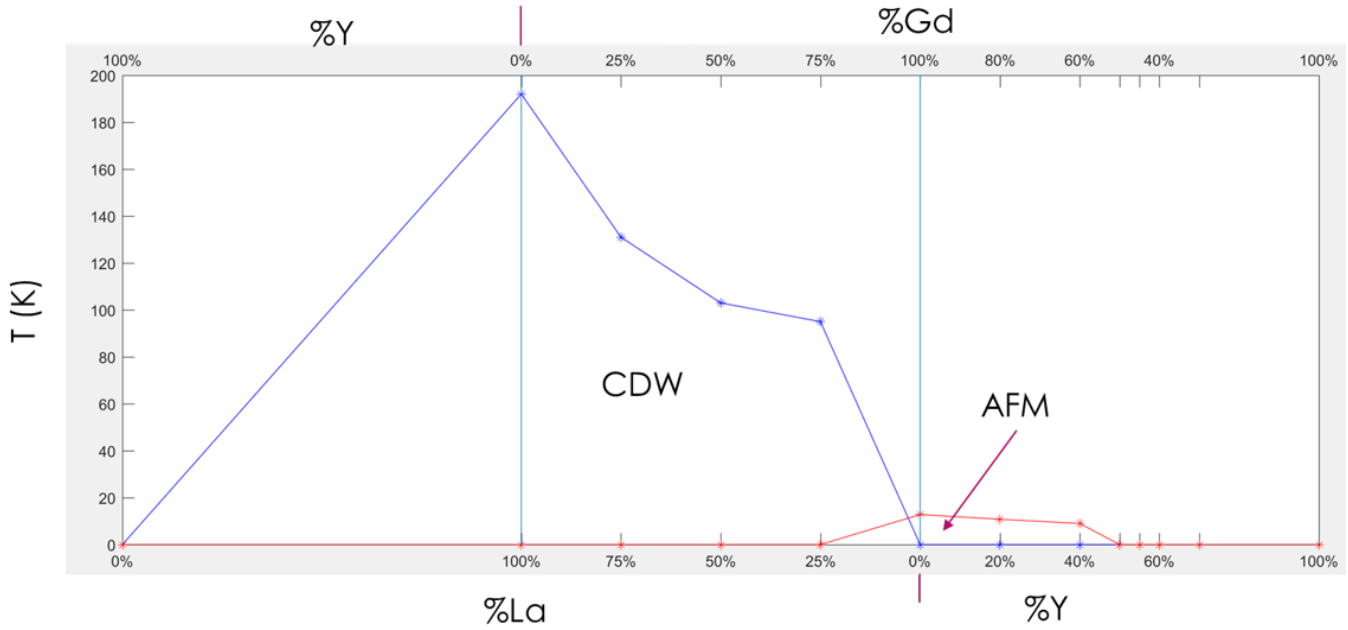

FIG. 7: Current measured crystals with observed phase transition temperatures. Further work can be done to resolve the quantum critical points where the charge density wave and antiferromagnetic states are suppressed in the La-Gd doping range, in addition to the measurement of crystals in the Y-La doping range.

in turn, the anomalous Nernst coefficient provides information about the energy derivative of the spin-resolved DOS at the Fermi level. The AHC of Fe_3GeTe_2 has been shown to be very large in Kim et. al. [11]. Additionally, Kim shows that this large AHC could not be induced by extrinsic mechanisms such as skew scattering or side jump, but instead is the result of an avoided band crossing in the DOS, which leads to a large Berry Curvature. This avoided band crossing should also result in a large anomalous Nernst coefficient and its measurement will provide additional information about the spin resolved DOS near the Fermi Level, giving a compelling reason for its measurement in Fe_3GeTe_2.

B. Measurement Techniques

The measurement of the Seebeck and Anomalous Nernst coefficients can be difficult, due to the characteristically small voltages (∼10 nV-10 μV) that are generated by reasonably attainable temperature gradients, which can often be saturated with large amounts of noise. Their detection often requires the use of a lock-in amplifier to filter out sources of noise. This can be accomplished by heating the substrate the sample sits on with a resistive heater driven with a sinusoidal current. Through the power law $P = I^2R$, this implies that the heating, ΔT is proportional to the following:

$$\Delta T \propto I^2(t)R \propto sin^2(\omega t) = \frac{1}{2}(1 - cos(2\omega t)), \quad (5)$$

where it is clear that the local heating will have a component at the second harmonic of the current drive. As both the Seebeck and anomalous Nernst voltages will be proportional to the temperature gradient generated, this means that both will have voltage components at the second harmonic and can be detected with a lock-in amplifier, providing the required experimental noise reduction.

The measured thermoelectric voltages, however, must be normalized by the temperature gradient in order to obtain thermoelectric coefficients and gain knowledge about the intrinsic properties of the material. Therefore, good knowledge of the temperature profile is required. This can be achieved by using a device design detailed in Peterson [9]. Reproduced in Fig. 8, this device consists of a metallic resistive heater on either side of the sample of interest and a metallic thermistor strip above it. With some normalization detailed in Peterson [9], the four thermistor contact points can be measured at the second harmonic to obtain the 2ω component of the local heating at their location, $\Delta T^{2\omega}(x)$. It is assumed here that Δ T is not a strong function of y, as ensured by the long length of the heaters with respect to the device. While this provides some information, and could be sufficient to normalize Seebeck voltages given proper contact placement, the localized temperature gradient at the point of the voltage measurements needs to be determined in the case of the anomalous Nernst coefficient. To do this, a model is developed to be fit to the thermistor data points. In principle, this could be done by solving

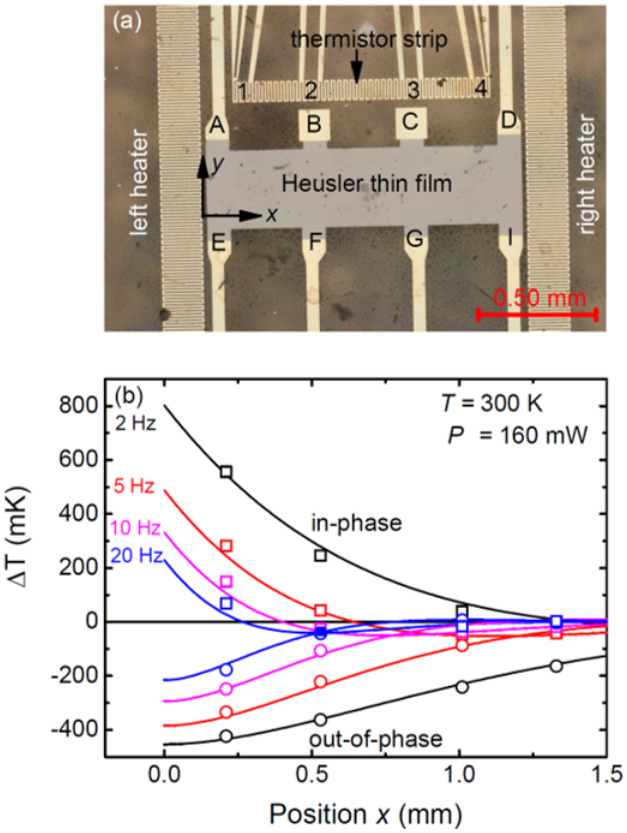

FIG. 8: (a) Device design used to measure (magneto)thermoelectric coefficients on epitaxial thin films, consisting of resistive heaters and a thermistor strip to characterize the temperature profile. Device fabrication is done using photolithography and e-beam metal evaporation. (b) Complex ΔT values for thermistors 1-4 as function of coordinate x taken from edge of the left heater. The squares are the in-phase with heater power quadrature while the circles are the out-of-phase quadrature, and data for several drive frequencies $\omega/2\pi$ are shown as indicated. Figure from Peterson [9].

the Heat Equation

$$f(\vec{r},t) = \frac{dT(\vec{r},t)}{dt} - D\nabla^2 T(\vec{r},t), \tag{6}$$

where D is the thermal diffusivity of the material and f($\vec{r}$,t) is an inhomogeneous source term representing the heaters. In the form of Eq. 6, the three dimensional heat equation is analytically intractable. As is shown in [9], this can be reduced to the one dimensional Helmholtz equation if some simplifying assumptions related to the device geometry are made, allowing one to obtain the following harmonic solution

$$\tilde{T}^{2\omega}(x,t) = A\frac{e^{-\left(\frac{r+i(2\omega)}{D}\right)^{\frac{1}{2}}|x|}}{2\left(\frac{r+i(2\omega)}{D}\right)^{\frac{1}{2}}}e^{i(2\omega)t}, \tag{7}$$

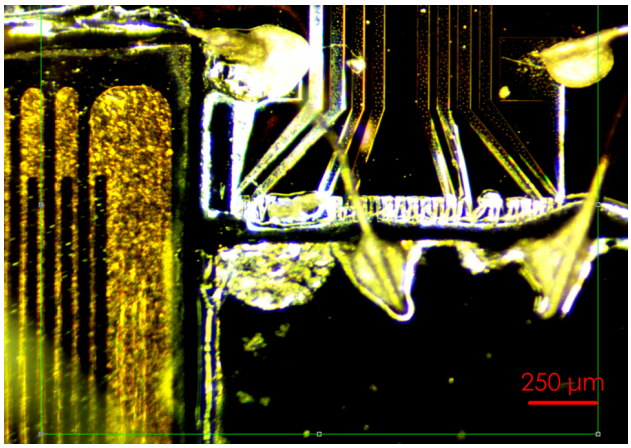

FIG. 9: Example of a modified (magneto)thermoelectric device for measurement of bulk crystals (compare to Fig. 8(a)). The main differences are that the crystal and drive heater are glued on the substrate and the crystal contacts are made with silver paste and wires rather than being patterned.

where r is a (phenomenological) relaxation term related to heat conduction through the substrate, and A is a constant related to the heater power and heat capacity of the system. The fits to Eq. 7 are shown in Fig. 8 (b), where the frequency dependence and phase sensitivity are exploited to increase the number of data points the model is fitting to. As can be seen in Fig. 8(b), this model has been successful in describing the temperature profile of epitaxial thin films grown on insulating substrates.

Despite past success, it is not immediately obvious that this model will extend to the bulk crystals of interest. One change that was necessary when measuring these crystals is that they need to be glued to the substrate as is shown in Fig. 9. Additionally due to some lithography related limitations, the heater element had to be glued on in this first iteration of devices rather than patterned (also in Fig. 9). These changes from the previously successful devices immediately raises two important questions: (1) will the larger thermal mass of the bulk crystal significantly affect heat conduction, which was assumed to be dominated by the substrate in Eq. 7? and (2) will the glued heater and crystal be in good enough thermal contact with the substrate for Eq. 7 to remain valid? The answer to the first of these questions is likely no, as although in the bulk, the crystal is still thin (∼10 μm) and almost certainly represents a significantly smaller thermal mass than the substrate (∼1 mm). There still might be some concern that the temperatures on the thermometer would be slightly different than that of those at the crystal surface due to the development of a vertical temperature gradient (∂_zT), but again the crystal is expected to be thin enough where this should not be an issue (albeit not as thin as the ∼10 nm epitaxial crystals). The answer to the second question is likely yes, as a variety of thermal glues exist specifically for

these types of applications. These potential issues still do deserve careful attention as measurements are taken even though they seem solvable. Specifically, from an experimental standpoint, success in fitting Eq. 7 and basic consistency checks (such as confirming that D derived from the fitting to Eq. 7 is in agreement with literature values for our substrate) would support the extension of this model to the slightly modified system. Numerical modeling of the system using finite element analysis could also be done in order to verify that the assumptions of the model in Eq. 7 are reasonable.

C. Preliminary Measurement Issues

Using the device in Fig. 9, we were unable to take a complete data set due to issues with the mounting of the crystal and heater on the substrate. A number of different adhesives were attempted for mounting, including Apiezon N Grease, silver paste, and Lakeshore GE Varnish. While each of these adhesives were successful in keeping the crystal and heater in thermal contact with the substrate (it was possible to measure second harmonic thermoelectric voltages and thermometer points), they all failed when cooled in a cryostat, loosing their adhesion and causing the crystal or heater to pop off and loose thermal contact. Additionally, the silver pasted wire contacts to the crystal would also pop off intermittently in the cryostat.

Even though no quantitative thermoelectric coefficients were measured due to these issues, this style of device holds promise due to its successful measurement of second harmonic thermoelectric voltages and thermometry data. As interesting DOS information is encoded in these thermoelectric coefficients and their successful measurement in Fe_3GeTe_2 may pave the way for future bulk crystals of interest, it is worth further investigation to solve these adhesion issues.

At present, a second iteration of the device in Fig. 9 is being fabricated in attempt to solve this issue. The main change is that Stycast thermally conductive epoxy will be used to keep the crystals secure. The heater was also able to be directly patterned on, which should improve its thermal contact and reduce the number of elements which could fail during the cooling. Additionally, more careful precautions will be taken to keep the substrate clean so that the adhesion between the crystal and substrate might be better. Finally, additional epoxy will be used to secure the wired contacts. If these extra steps are successful in securing the crystal and wires, the next step would be to fit the measured thermometry data to Eq. 7, which if successful, will allow one to derive thermoelectric coefficients from the measured voltages.

IV. CONCLUSION

In section II, the phase diagram of $RAgSb_2$ was explored due to the known CDW and AFM states in the La and Gd based parent compounds respectively, which may result in a SC phase related to their suppression. As these states are suppressed with doping, this was expected to create a QCP similar to that in superconducting cuprates such as YBCO, as shown in figures 2 and 3. Y doping on $RAgSb_2$ was also preformed to create a QCP with its metallic paramagnet phase, which could create an SC phase as well. While no SC phase has been measured for $RAgSb_2$ yet, as shown in Fig. 7, there are still many additional doping measurements that need to be preformed to complete the phase diagram, especially near the suppression of AFM and CDW states in $La_xGd_{1-x}AgSb_2$. These additional doping measurements should be able to resolve the QCPs of $La_xGd_{1-x}AgSb_2$ or potentially reveal something different such as a first order quantum phase transition or coexistence of states. Even if no SC phase, or further QCPs are found, we will have learned more about the conditions necessary for SC to arise in materials such as cuprates, which could aid the development of a non-BCS SC theory.

In section III, a device and technique was introduced that allows for the measurement of thermoelectric coefficients of thin film ($\sim$ 10 nm) epitaxial crystals. With slight modification, we expect this measurement technique will extend to work for bulk grown crystals. At the time of writing, the extension of this measurement technique could not be verified due to issues mounting the crystal to the substrate. Once this issue is resolved, we will be able to see if this measurement technique does extend to bulk crystals. If so, it will allow one to gain valuable information about the band structure of Fe_3GeTe_2 through the thermoelectric coefficient measurements, and would also pave the way for future measurement of bulk crystals as well.

V. ACKNOWLEDGEMENTS

I would like to give a special thanks to the National Science Foundation for making this research experience possible. I would also like to thank University of Washington REU program directors Deep Gupta, Gray Rybka, Linda Vilett and Cheryl McDaniel. Finally, I would like to thank Professor Jiun-Haw Chu and the members of his Quantum Materials Lab for an enjoyable summer.

[1] N. Doiron-Leyraud, C. Proust, D. LeBoeuf, J. Levallois, J.-B. Bonnemaison, R. Liang, D. A. Bonn, W. N. Hardy, and L. Taillefer, Nature **447**, 565 EP (2007).

[2] B. J. Ramshaw, S. E. Sebastian, R. D. McDonald, J. Day, B. S. Tan, Z. Zhu, J. B. Betts, R. Liang, D. A. Bonn, W. N. Hardy, and N. Harrison, Science **348**, 317 (2015),

http://science.sciencemag.org/content/348/6232/317.full.pdf.

[3] O. Cyr-Choinire, D. LeBoeuf, S. Badoux, S. Dufour-Beausjour, D. A. Bonn, W. Hardy, R. Liang, N. Doiron-Leyraud, and L. Taillefer, (2015).

[4] K. Myers, S. Bud'ko, I. Fisher, Z. Islam, H. Kleinke, A. Lacerda, and P. Canfield, Journal of Magnetism and Magnetic Materials **205**, 27 (1999).

[5] N. Barii, M. K Chan, Y. Li, G. Yu, X. Zhao, M. Dressel, A. Smontara, and M. Greven, *Proceedings of the National Academy of Sciences of the United States of America*, **110** (2013).

[6] G. Campi, A. Ricci, N. Poccia, M. Fratini, and A. Bianconi, *Condensed Matter*, **2** (2017).

[7] X. F. Wang, T. Wu, G. Wu, R. H. Liu, H. Chen, Y. L. Xie, and X. H. Chen, New Journal of Physics **11**, 045003 (2009).

[8] Y. Muro, N. Takeda, and M. Ishikawa, Journal of Alloys and Compounds **257**, 23 (1997).

[9] T. A. Peterson, Ph.D. Thesis, University of Minnesota (2018).

[10] D. Xiao, Y. Yao, Z. Fang, and Q. Niu, Phys. Rev. Lett. **97**, 026603 (2006).

[11] K. Kim, J. Seo, E. Lee, K.-T. Ko, B. S. Kim, B. G. Jang, J. M. Ok, J. Lee, Y. J. Jo, W. Kang, J. H. Shim, C. Kim, H. W. Yeom, B. Il Min, B.-J. Yang, and J. S. Kim, Nature Materials (2018), 10.1038/s41563-018-0132-3.